Multiphoton processes in the presence of self-phase-modulation

Oscar G. Calderón* and Alan H. Chin†
W. W. Hansen Experimental Physics Laboratory, Stanford University, Stanford, California 94305

Junichiro Kono
Department of Electrical and Computer Engineering, Rice University, Houston, Texas 77005
(Received 24 August 2000; published 13 April 2001)

We have theoretically investigated the effects of self-phase-modulation on multiphoton nonlinear optical processes in semiconductors, utilizing multiple-order perturbation theory based on a set of coupled nonlinear-wave equations. Our results clearly demonstrate that the self-phase-modulation in the fundamental field induces spectral broadening in the harmonic fields (cross-phase modulation) and alleviates phase mismatch by providing a distribution of wave vectors. These results are consistent with our recent observation of extreme nonlinear optical behavior in bulk semiconductors under intense mid-infrared radiation.

DOI: 10.1103/PhysRevA.63.053807 PACS number(s): 42.65.Ky, 42.65.Re, 42.70.Nq, 42.65.Hw

I. INTRODUCTION

Self-phase-modulation (SPM) is a fundamental nonlinear optical process, which, in combination with self-focusing, is known to lead to dramatic continuum generation when a high-intensity ultrafast laser pulse is focused into a stable filament [1]. This extreme case of SPM has been observed in many different types of materials and gases [2,3] and is used for generating ultrafast radiation outside the conventional spectral range of ultrafast lasers for various applications [4]. Although there have been a number of studies on SPM and continuum generation [5–7], the effect of SPM on multiphoton processes is less well understood [8].

In this paper, we theoretically study the effect of SPM on multiple-order nonlinear optical processes. Specifically, we investigate multiple-harmonic generation and (off-resonance) multiple optical sideband generation processes that have recently been observed in bulk semiconductors strongly driven by intense mid-infrared (MIR) laser pulses [9]. Multiple-harmonic generation in gases, liquids, and solid surfaces in both perturbative and nonperturbative regimes has been well explored [10–13], but there have been few studies in *bulk* solids. The importance of SPM via cross-phase-modulation (XPM) in harmonic generation [8,14,15], wave mixing [16], and pairs of copropagating beams [17] has been considered, but the importance of SPM in *multiple-order* nonlinear processes has not been fully addressed, to our knowledge.

We have developed a multiple-order perturbation theory based on a set of coupled nonlinear-wave equations. We find that spectral broadening in the harmonic fields occurs due to XPM, i.e., spectral broadening of the fundamental beam being mapped onto the harmonic during propagation [18]. We also find that multiple-sideband generation and multiple-harmonic generation are significantly enhanced by SPM. This is because the additional bandwidth in the fundamental due to SPM provides a distribution of wave vectors, which in turn help alleviate any strong thickness dependence due to phase mismatch. Our numerical simulations agree well with the observations in Ref. [9].

This paper is organized as follows. The theory used to describe multiple-order nonlinear processes in the presence of SPM is described in Sec. II. In that section, we first develop the coupled nonlinear-wave equations using multiple-order perturbation theory (Sec. II A) and analyze harmonic spectral broadening (Sec. II B). We then consider multiple-order nonlinear phenomena in the presence of SPM for the case of harmonic generation (Sec. II C) and for the case of off-resonance sum and difference frequency generation, which we call sideband generation (Sec. II D). Comparison of the theoretical results with the experiments is shown in Sec. III, and conclusions are stated in Sec. IV.

II. THEORY

A. Nonlinear-wave equation

Our theoretical study of multiple-order nonlinear-optical phenomena is based on the standard nonlinear-wave equation formalism [19]. For the pulse propagation of a field A_j, with frequency ω_j, the wave equation is

$$\frac{\partial A_j(z,\xi)}{\partial z} = i\frac{2\pi\omega_j}{cn_0}P^{(+)}_{NLj}(z,\xi). \tag{2.1}$$

In Eq. (2.1) we have used the slowly varying envelope approximation for the field $E_j = A_j \exp[i(k_j z - \omega_j t)] + \text{c.c.}$, where $k_j = n_0(\omega_j)\omega_j/c$, and for the nonlinear polarization $P_{NL} = \chi^{(2)}E^2 + \chi^{(3)}E^3 + \ldots = P^{(+)}_{NLj}\exp[i(k_j z - \omega_j t)] + \text{c.c.}$ $\xi \equiv t - z/(c/n_0)$ is a reduced time scale [20].

We first study the propagation of the fundamental field $(E_1,\ \omega_1)$ which propagates through a nonlinear medium with an index of refraction that depends on intensity by means of the third-order contribution of the nonlinear polarization $P^{(+)}_{NL1} = 3\chi^{(3)}|A_1|^2 A_1$. The solution is

*Permanent address: Departamento Optica, Universidad Complutense de Madrid, Ciudad Universitaria s/n, 28040 Madrid, Spain.
†Present address: Information Science & Technology Division, Lawrence Livermore National Laboratory, Livermore, CA 94551.

$$A_1(z,\xi)=|A_1(0,\xi)|\exp\left(i\frac{4n_2\omega_1}{c}|A_1(0,\xi)|^2z\right), \quad (2.2)$$

where $n_2\equiv 3\pi\chi^{(3)}/(2n_0)$ is the nonlinear index of refraction. Equation (2.2) represents a pulse whose intensity does not change but whose phase changes during propagation. This phase shift occurs due to SPM, and the amount of phase shift ϕ_1 after a distance L is given by

$$\phi_1=\frac{4n_2\omega_1}{c}|A_1|^2L. \quad (2.3)$$

Since the intensity $|A_1|^2$ varies throughout the pulse ($|A_1|^2$ is a function of ξ), various parts of the pulse undergo different phase shifts, leading to a frequency shift. We assume the boundary condition for the fundamental field to be $A_1(0,t)^2=A_0^2/\cosh(t/T)$, where T is related to the pulse duration Δ by $T\equiv\Delta/[2\ \mathrm{arccosh}(2)]$, and A_0 to the pulse intensity I_0 by $A_0^2\equiv 4\ \mathrm{arccosh}(2)I_0/(n_0c)$. After the pulse travels a distance L in the medium, the difference between its instantaneous optical frequency [at time $t+L/(c/n_0)$] and the carrier frequency ω_1 is obtained by differentiating the phase shift with respect to t [20]:

$$\delta\omega_1=-\frac{d\phi_1}{dt}=\frac{4n_2\omega_1L}{c}\frac{A_0^2}{T}\frac{\sinh(t/T)}{\cosh^2(t/T)}. \quad (2.4)$$

Assuming $n_2>0$, the instantaneous frequencies in the leading half of the pulse are lowered, whereas those in the trailing half are raised. The total frequency excursion is $2(\delta\omega_1)_{max}=4n_2\omega_1LA_0^2/(cT)$.

B. Harmonic spectral broadening

In this section, we study how the spectral broadening in the harmonic field takes place. We consider third-harmonic generation induced by the fundamental field via the third-order nonlinear susceptibility, since all media have nonzero $\chi^{(3)}$. Its corresponding third-order nonlinear polarization is given by

$$P_{NL3}^{(+)}=\chi^{(3)}[A_1^3e^{-i\Delta kz}+6|A_1|^2A_3+3|A_3|^2A_3], \quad (2.5)$$

where A_3 is the third-harmonic field ($\omega_3=3\omega_1$) and $\Delta k\equiv k_3-3k_1$ the phase mismatch. We approximately solve the propagation of the harmonic field (A_3), taking into account that $|A_1|^2\gg|A_3|^2$ so that we can neglect the smallest term of the nonlinear polarization, $3|A_3|^2A_3$. Then, using the fundamental field A_1 calculated in Sec. II A, we solve the propagation equation of the third-harmonic field

$$\frac{\partial A_3}{\partial z}=i\frac{4n_2\omega_1}{c}[A_1^3e^{-i\Delta kz}+6|A_1|^2A_3]. \quad (2.6)$$

The wave equation is a linear differential equation, whose solution at $z=L$ is

$$A_3=\frac{|A_1|}{3}\frac{1}{1+\Delta kL/3\phi_1}[e^{i6\phi_1}-e^{i(3\phi_1-\Delta kL)}]. \quad (2.7)$$

TABLE I. Parameters for the spectral broadening in the third harmonic in GaAs.

$n_0(\omega_1)$	$n_0(\omega_3)$	$\chi^{(3)}$ (esu)
3.311	3.4345	3.1×10^{-11}

The intensity of the third harmonic is modulated by the phase of the fundamental field, $|A_3|^2\propto 1-\cos(3\phi_1+\Delta kL)$. Thus, the third-harmonic pulse (when $\phi_1\simeq 0$) suffers a modulation as well as spectral broadening due to SPM. As we will see in the numerical example given below, this intensity modulation of the harmonic is evident as a slow modulation of its energy spectrum. The third-harmonic pulse also experiences a phase shift ϕ_3 induced by the SPM of the fundamental field

$$\phi_3=\arctan\left[\frac{\sin(6\phi_1)-\sin(3\phi_1-\Delta kL)}{\cos(6\phi_1)-\cos(3\phi_1-\Delta kL)}\right]. \quad (2.8)$$

After the pulse has traveled a distance L in the medium, the difference between its instantaneous optical frequency and the carrier frequency ω_3 is $\delta\omega_3=(9/2)\delta\omega_1$. Therefore its relative frequency shift is

$$\frac{\delta\omega_3}{\omega_3}=\frac{3}{2}\frac{\delta\omega_1}{\omega_1}. \quad (2.9)$$

This shows that the relative frequency shift of the harmonic field is greater than the fundamental frequency shift, with the total frequency excursion for the harmonic field given by $2(\delta\omega_3)_{max}=(9/2)2(\delta\omega_1)_{max}$. The broadening found in the harmonic field is due to the spectral broadening of the fundamental beam, generated by SPM, being mapped onto the harmonic during propagation via XPM, i.e., no significant SPM due to the harmonic beam itself is generated.

Numerical example

Let us consider a high intensity ($I_0\simeq 10^{11}$ W/cm^2) using $\Delta=200$ fs pulses at $\lambda_1=3.5$ μm in an $L=350$ μm thick crystal. The linear index of refraction and the nonlinear susceptibility used are shown in Table I. Figure 1(a) shows the calculated third-harmonic intensity using the parameter stated above. Here we see how the SPM modifies the pulse shape of the third harmonic. This intensity modulation is induced by the changing phase of the fundamental field due to SPM. Figure 1(b) shows the calculated relative frequency shift for both fields, the fundamental field (dotted line) and the third harmonic (solid line). Due to this time-varying phase, the spectrum of the transmitted pulse is modified, with more broadening occurring in the third-harmonic [see Eq. (2.9)]. This is clearly seen in Fig. 1(c), which shows the spectral content of the transmitted pulse calculated using

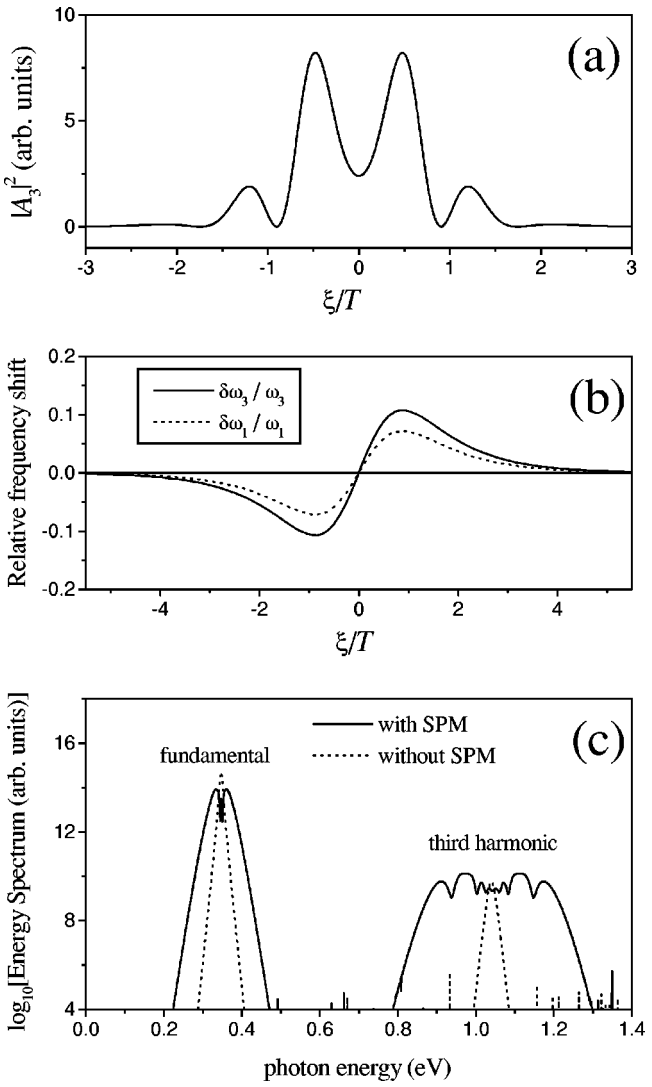

FIG. 1. (a) Calculations for 350 μm thick GaAs. Intensity of the third harmonic field $|A_3|^2$ at $z=L$, as a function of pulse position ξ/T. (b) Relative frequency shift for the fundamental field $\delta\omega_1/\omega_1$ (dotted line) and for the third-harmonic field $\delta\omega_3/\omega_3$ (solid line) versus the pulse position ξ/T at $z=L$. (c) Energy spectra of the fundamental and third-harmonic fields calculated with SPM (solid line) and without SPM (dotted line), demonstrating harmonic spectral broadening when SPM is taken into account.

$$S(\omega)=\left|\int_{-\infty}^{\infty}dte^{i\omega t}(|A_1|e^{i\phi_1}e^{i(k_1z-\omega_1t)}+|A_3|e^{i\phi_3}e^{i(k_3z-\omega_3t)})\right|^2. \tag{2.10}$$

The dotted line in this figure corresponds to the case without SPM and is shown to highlight the spectral broadening due to SPM. Figure 2 shows the energy spectrum in the third harmonic and its total energy versus thickness, with and without SPM. The two cases follow different phase-matching behavior, as will be addressed in next subsection. Since SPM is a nonlinear process, the espectral broadening should be strongly intensity dependent. Figure 3 shows the

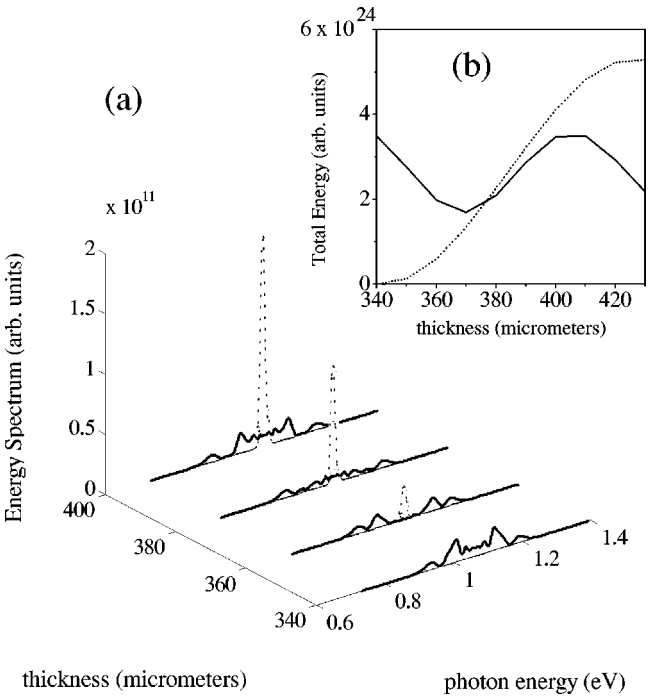

FIG. 2. Theoretical (a) energy spectrum and (b) total energy of the third harmonic in GaAs versus thickness, with SPM (solid line) and without SPM (dotted line).

energy spectrum in the third harmonic for both intensities I_0 and $I_0/2$. We find that both the overall spectral width and the intensity of the peaks become smaller as the pulse intensity decreases.

C. Multiple-harmonic generation

The previous subsection highlighted the effect of XPM on a single harmonic. Here we analyze the multiple-harmonic generation with XPM. We assume that the primary mechanism responsible for harmonic generation is the direct process, so that all of the cross terms are negligible. Then, the nonlinear polarization for the harmonic field A_j ($j=2,3,\ldots$) at frequency $\omega_j=j\omega_1$ is related to the fundamental field A_1 by

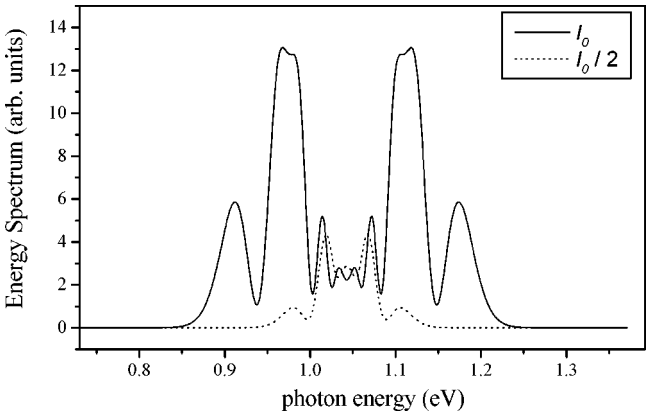

FIG. 3. Theoretical energy spectrum in the third harmonic in GaAs for different pulse intensities I_0 (solid line) and $I_0/2$ (dotted line).

$$P_{NLj}^{(+)}=\chi^{(j)}(A_1)^j e^{-i\Delta k_j z}, \tag{2.11}$$

where $\Delta k_j=k_j-jk_1$ is the phase mismatch and $\chi^{(j)}$ is the jth-order nonlinear susceptibility. Introducing Eq. (2.2) into Eq. (2.11), we can solve the propagation equation for the harmonic field [Eq. (2.1)] after a distance L,

$$A_j=i\frac{2\pi\omega_j L\chi^{(j)}}{cn_0}|A_1|^j \operatorname{sinc}\left[\frac{j\phi_1-\Delta k_j L}{2}\right]e^{i(j\phi_1-\Delta k_j L)/2}, \tag{2.12}$$

where $\operatorname{sinc}(x)\equiv\sin(x)/x$. This solution predicts that harmonics have the standard perturbative behavior with the fundamental intensity: $|A_j|^2\propto|A_1|^{2j}$.

In order to understand the role played by XPM in harmonic generation, we first review the case without SPM in the fundamental, i.e., $\phi_1\simeq 0$. In this case, the harmonic intensity is proportional to the well known function $\operatorname{sinc}^2(\Delta k_j L/2)$. The distance where the polarization wave at ω_j and light wave at ω_j remains in phase synchronism is called the interaction length (or coherence length), and is defined as $l_c\equiv\pi/(k_j-jk_1)=\lambda_1/[2j|n_0(\omega_j)-n_0(\omega_1)|]$ [20]. We see that $l_c\propto\lambda_1$ and thus longer wavelengths generally lead to larger interaction lengths. When this distance is much shorter than the thickness of the sample, a large phase mismatch occurs, and the intensity becomes very sensitive to the sample length, as illustrated in Fig. 4(a). This leads to a strong reduction of the harmonic fields if the sinc function is close to zero. However, if we consider SPM in the fundamental, the argument of the sinc function will be equal to $(\Delta k_j L-j\phi_1)/2$ (due to XPM), instead of $(\Delta k_j L/2)$. Consequently, SPM aids phase matching by generating a large distribution of wave vectors, which averages out any destructive interference. An example of how much influence SPM can have on the phase matching is shown in Fig. 4(b). Therefore, the additional bandwidth in the fundamental due to SPM alleviates any strong thickness dependence due to phase mismatch by providing a distribution of wave vectors, as is seen in Fig. 2.

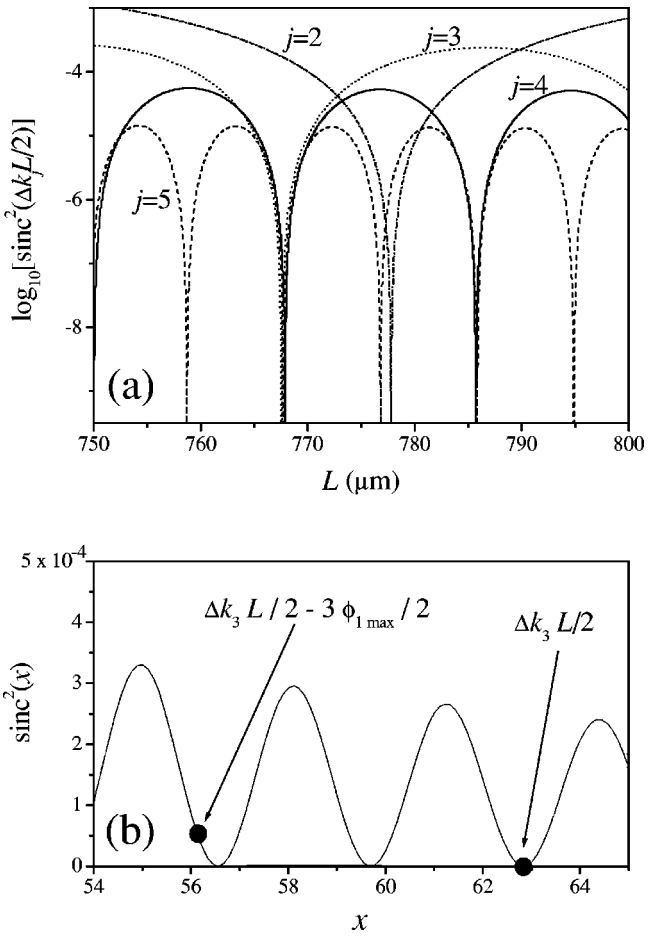

FIG. 4. (a) Plot of the phase matching condition (without SPM) versus ZnS thickness for the different harmonic fields: second harmonic (dotted and dashed line), third harmonic (dotted line), fourth harmonic (solid line), and fifth harmonic (dashed line). (b) Plot of the phase matching condition for third-harmonic generation for the conditions mentioned in the text. The values correspond to the cases without SPM, $x=\Delta k_3 L/2$, and the maximum change when SPM is considered, $x=\Delta k_3 L/2-3\phi_{1\max}/2$, are shown. The whole range of phase matching between these points is achieved when SPM occurs, thereby averaging out the effect of phase mismatch.

Numerical example

To demonstrate the effect of XPM, consider a $\Delta=1$ ps pulse with a peak intensity $I_0\simeq 2\times10^{10}$ W/cm^2 at wavelength $\lambda_1=3.5$ μm. The linear index of refraction and the nonlinear susceptibilities used are shown in Table II. Using these parameters, the estimated interaction length for generating harmonics is on the order of 20 μm. For a 1 mm thick sample this leads to a large phase mismatch. Figure 4(a) shows the standard sinc function (without SPM) versus the thickness (L) for different harmonics. Around $L\simeq 768$ μm the third, fourth, and fifth harmonics are strongly suppressed due to phase mismatch between the fundamental and the harmonics. We calculate the energy spectrum

$$S(\omega)=\left|\int_{-\infty}^{\infty}dt\, e^{i\omega t}\sum_j A_j e^{i(k_j z-\omega_j t)}\right|^2 \tag{2.13}$$

for both cases, with and without SPM at $L=768$ μm. Plotted in Fig. 5 is the resulting energy spectrum, which demonstrates that multiple harmonics do not appear for this case without SPM. In order to show how SPM alleviates any strong thickness dependence of the phase matching we plot in Fig. 4(b) the sinc function around the third-harmonic position. As we can see in this figure, the sinc function is close to a zero for the third-harmonic phase matching. However, the SPM provides a distribution of wave vectors that averages out any destructive interference (see Fig. 2 for this ef-

TABLE II. Parameters for the MIR harmonics in ZnS.

$\chi^{(2)}$ (esu)	$\chi^{(3)}$ (esu)	$\chi^{(4)}$ (esu)	$\chi^{(5)}$ (esu)	
0.8×10^{-7}	5×10^{-11}	4.2×10^{-15}	6.5×10^{-19}	
$n_0(\omega_1)$	$n_0(\omega_2)$	$n_0(\omega_3)$	$n_0(\omega_4)$	$n_0(\omega_5)$
2.2545	2.268	2.2849	2.3035	2.332

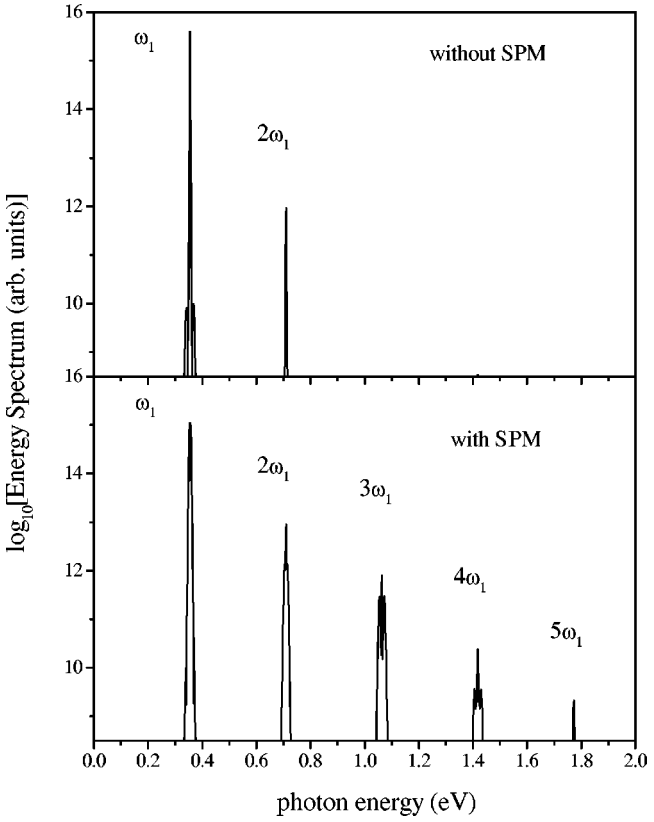

FIG. 5. Theoretical energy spectrum of the total field corresponding to multiple-harmonic generation in ZnS, with and without SPM.

fect in GaAs). This allows the generation of multiple harmonics to occur more easily, as seen in Fig. 5.

An interesting situation occurs when we consider the zero dispersion limit, i.e., $\Delta k_j \simeq 0$. In this case, there is a phase mismatch generated by SPM and therefore the intensity of the harmonics generated with SPM will decrease with respect to the case without SPM (although the spectrum is broader with SPM). This is shown in Fig. 6, where we plot the calculated third-harmonic energy spectrum with and without SPM assuming zero dispersion.

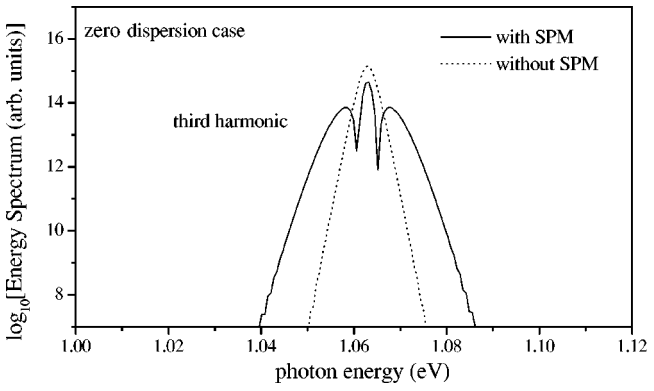

FIG. 6. Theoretical third-harmonic energy spectrum in a material with zero dispersion, $\Delta k_3 = 0$, with SPM (solid line) and without SPM (dotted line). The parameters are the same as in Fig. 5, but with a shorter length $L = 200\ \mu$m.

D. Multiple-sideband generation

Another nonlinear phenomenon that can be affected by SPM is sideband generation, i.e., sum and difference frequency generation. In this subsection, we study the optical sidebands generated when the fundamental field A_1 [Eq. (2.2)] and a probe pulse A_p (frequency ω_p) overlap. We consider a probe pulse as follows: $A_p(z,\xi)^2 = A_{0p}^2/\cosh(\xi/T_p)$, where $T_p \equiv \Delta_p/[2\,\mathrm{arccosh}(2)]$, with Δ_p the pulse duration, and $A_{0p}^2 \equiv 4\,\mathrm{arccosh}(2) I_{0p}/(n_0 c)$, with I_{0p} the pulse intensity. The two fields propagate with a small relative angle θ. If we take the fundamental field in the propagation direction, i.e. the z axis, the probe wave vector direction is given by $\vec{k}_p = k_p[\cos(\theta)\hat{z} + \sin(\theta)\hat{x}]$. We analyze the sum and difference frequencies ($\omega_{\pm 1} = \omega_p \pm \omega_1$), and higher-order wave mixing ($\omega_{\pm j} = \omega_p \pm j\omega_1$). The corresponding nonlinear polarization for these processes is

$$P_{NL\pm j}^{(+)} = (j+1)\chi^{(j+1)} A_p |A_1|^j \times \exp\left(\pm j i \frac{4 n_2 \omega_1 |A_1|^2}{c} z\right) \exp(i \Delta k_{\pm j} z), \tag{2.14}$$

where

$$\Delta k_{\pm j} = (\hat{z}\cdot\vec{k}_p) \pm j k_1 - (\hat{z}\cdot\vec{k}_{\pm j}) \tag{2.15}$$

is the phase mismatch. Using this nonlinear polarization [Eq. (2.14)] we solve the wave equation [Eq. (2.1)] after a distance L,

$$A_{\pm j} = i \frac{2(j+1)\pi \omega_{\pm j} L \chi^{(j+1)}}{n_0 c} A_p |A_1|^j \,\mathrm{sinc} \times \left[\frac{\pm j \phi_1 + \Delta k_{\pm j} L}{2}\right] e^{i(\pm j \phi_1 + \Delta k_{\pm j} L)/2}. \tag{2.16}$$

This solution gives the standard perturbative behavior, i.e., ± 1 (± 2) photon sidebands are linearly (quadratically) dependent on the fundamental intensity, $|A_{\pm j}|^2 \propto |A_1|^{2j}$, and linearly dependent on the probe intensity, $|A_{\pm j}|^2 \propto |A_p|^2$. As with multiple-harmonic generation, the SPM avoids any strong thickness dependence due to phase matching in the sideband generation.

Numerical example

Let us consider the following parameters: a probe pulse ($\lambda_p = 0.8\ \mu$m) with peak intensity $I_p \simeq 1\times 10^9$ W/cm^2 and $\Delta_p = 1$ ps, interacting with a $\Delta = 1$ ps pulse of wavelength $\lambda_1 = 3.5\ \mu$m with peak intensity $I_0 \simeq 2\times 10^{10}$ W/cm^2. The angle between the probe and the fundamental field is $\theta = 10°$. The linear index of refraction and the nonlinear susceptibilities used are shown in Table III. The effective length is $L = 489\ \mu$m, which is the length over which the beams are crossed on the sample. In order to show the sideband generation we calculate the energy spectrum

TABLE III. Parameters for the optical sidebands in ZnSe.

	$n_0(\omega_p)=2.5244$	
$\chi^{(2)}=6\times10^{-7}$ esu	$\chi^{(3)}=8.5\times10^{-11}$ esu	$\chi^{(4)}=6\times10^{-15}$ esu
	$\lambda_1=3.5\ \mu$m	$n_0(\omega_1)=2.4352$
$n_0(\omega_{+1})=2.5815$	$n_0(\omega_{+2})=2.6655$	
$n_0(\omega_{-1})=2.4866$	$n_0(\omega_{-2})=2.4588$	
	$\lambda_1=6.2\ \mu$m	$n_0(\omega_1)=2.4251$
$n_0(\omega_{+1})=2.5536$	$n_0(\omega_{+2})=2.5899$	$n_0(\omega_{+3})=2.6347$
$n_0(\omega_{-1})=2.5005$	$n_0(\omega_{-2})=2.4837$	$n_0(\omega_{-3})=2.4676$

$$S(\omega)=\left|\int_{-\infty}^{\infty}dt e^{i\omega t}\left\{A_p e^{i[(\hat{z}\cdot\vec{k}_p)z-\omega_p t]}+A_1 e^{i(k_1 z-\omega_1 t)}+\sum_j A_{+j}e^{i[(\hat{z}\cdot\vec{k}_{+j})z-\omega_{+j}t]}+\sum_j A_{-j}e^{i[(\hat{z}\cdot\vec{k}_{-j})z-\omega_{-j}t]}\right\}\right|^2 \quad (2.17)$$

for both cases, with and without SPM. As we can see in Fig. 7, the sidebands are strongly affected by the phase matching effect when the SPM is not taken into account.

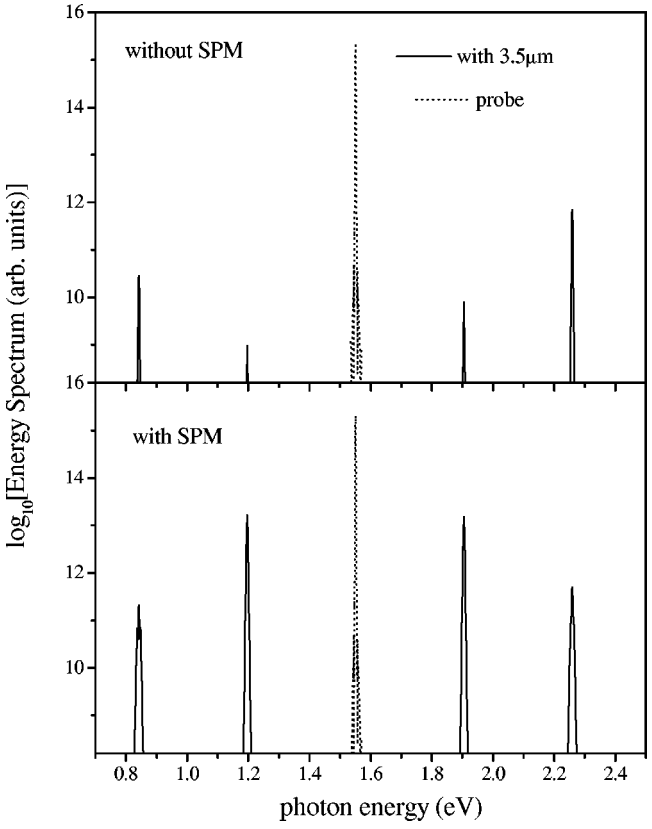

FIG. 7. Theoretical energy spectrum of the total field corresponding to multiple-sideband generation in ZnSe, with and without SPM.

III. COMPARISON WITH EXPERIMENTAL MULTIPLE-ORDER NONLINEAR OPTICAL PHENOMENA

In this section, we compare the theoretical results with recent experiments in multiple-order nonlinear optical phenomena induced by intense MIR pulses in semiconductors [9]. In this work, we observed both multiple harmonics and multiple sidebands. In addition, we observed unusual spectral modulation in a harmonic under high-intensity conditions, which is not directly addressed by the theory stated above.

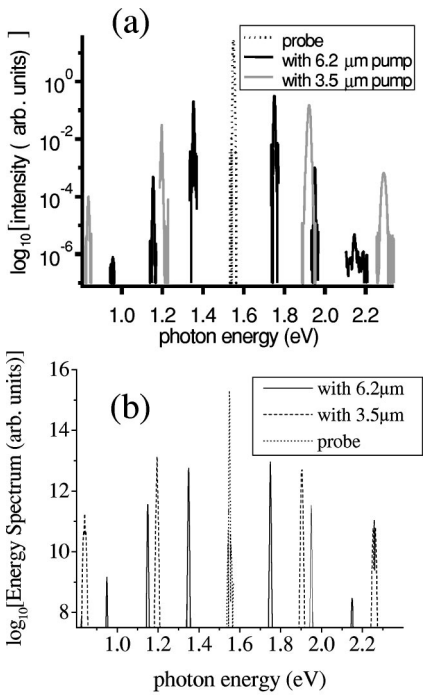

FIG. 8. (a) Optical sidebands in polycrystalline ZnSe (3 mm thick) generated when a MIR pump pulse ($\simeq$1 ps) and a 800 nm (1.55 eV) probe pulse (dotted curve) are overlapped. The sidebands generated by 3.5 μm (gray curves) and 6.2 μm (black curves) MIR are shown. (b) Theoretical energy spectrum of the total field corresponding to the optical sideband generation for the same parameters.

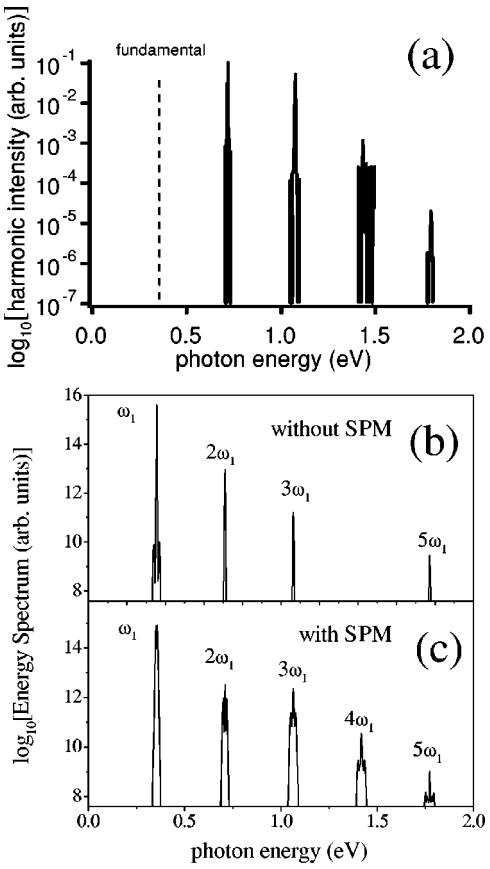

FIG. 9. (a) MIR harmonics in polycrystalline ZnS (2 mm thick) using 3.5 μm, $\simeq$1 ps MIR pulses. Theoretical energy spectrum of the total field corresponding to the MIR harmonics, (b) without and (c) with SPM, for the same parameters.

In the previous experimental work [9], we observed multiple MIR harmonics below the band edge in semiconductors. Figure 9(a) shows the multiple harmonics observed in polycrystalline ZnS (2 mm thick) using 3.5 μm (0.35 eV), $\simeq$1 ps MIR pulses with a peak intensity of $\simeq 2\times10^{10}$ W/cm^2. The estimated phase matching interaction length taking into account the dispersion (using values in Table II) ranges from $\simeq$60 μm for the second harmonic to $\simeq$5 μm for the fifth harmonic and are much shorter than the thickness of the samples ($\simeq$1 mm). This should lead to a strong dependence on the phase mismatch that leads to a strong dependence on sample thickness. However, this strong dependence is alleviated by SPM, as discussed above. The theoretical spectrum corresponding to these experimental values is shown in Fig. 9 neglecting SPM [Fig. 9(b)] and taking SPM into account [Fig. 9(c)]. Good agreement between the calculations with SPM and the data is obtained. We see how the fourth harmonic is not present in the energy spectrum when SPM is not taken into account. That means that the mismatch for the fourth harmonic, $\Delta k_4 L/2$, is close to a zero of the sinc function. This strong reduction of the harmonic is alleviated by the additional phase matching generated by SPM. Up to the maximum MIR intensity using the picosecond pulses, the second, third, and fourth harmonics are measured to have quadratic, cubic, and quartic dependence with the MIR intensity, respectively. This is the standard perturbative behavior predicted by the theoretical model, even under these high-intensity conditions.

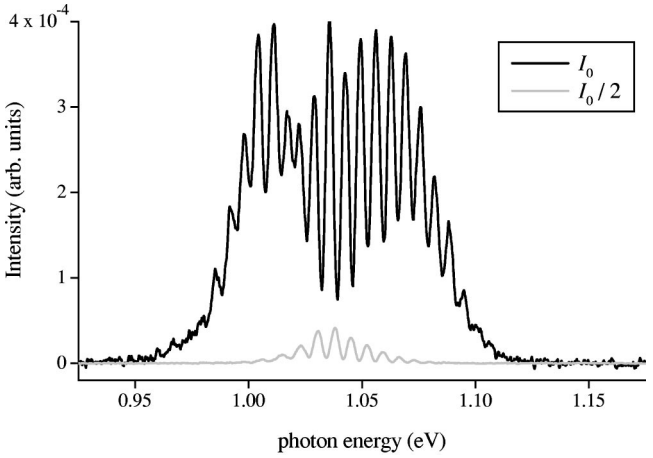

FIG. 10. Spectral broadening in the third harmonic of 3.5 μm, $\simeq$200 fs MIR in 350 μm thick GaAs(100), using $I_0\simeq10^{11}$ W/cm^2 (black) and $I_0/2$ (gray).

In addition to multiple harmonics, we also observed multiple sidebands by measuring the near-infrared (NIR) spectrum after mixing of intense NIR and MIR beams in a semiconductor [9]. As shown in Fig. 8(a) the NIR probe pulse spectrum (1.55 eV) is significantly modified to possess sidebands that are spaced by the MIR photon energy. The two sets of data in Fig. 8(a) were obtained in polycrystalline ZnSe (effective length $L\simeq500$ μm at $\theta=10°$) using $\simeq$1 ps pulses of either 3.5 μm wavelength (0.35 eV) with peak intensity of $\simeq2\times10^{10}$ W/cm^2 or 6.2 μm wavelength (0.22 eV) with peak intensity of $\simeq3\times10^{9}$ W/cm^2. The theoretical spectrum corresponding to this case (using values of Table III) is shown in Fig. 8(b). Good agreement between the calculations and the data is obtained. The ±1 (±2) MIR photon sidebands are linearly (quadratically) dependent on the MIR intensity up to the maximum MIR intensity used in these experiments, following the perturbative behavior expected by our theoretical model. Also, all of the sidebands are linearly dependent on the NIR intensity. From Fig. 8(a) or 8(b), we can see that the sidebands generated by both MIR fields (3.5 μm and 6.2 μm) have similar intensity values. This may be surprising, because the 6.2 μm pulse intensity is close to one order of magnitude smaller than the 3.5 μm pulse. However, the intensity value in the energy spectrum of each sideband depends on the phase matching condition. Thus, the longer wavelength (6.2 μm) allows better phase matching, which compensates for the smaller pulse intensity.

The data presented above is consistent with our theoretical model. However, with higher MIR intensity ($\simeq10^{11}$ W/cm^2) using $\simeq$200 fs pulses at 3.5 μm, an interesting broadening with spectral modulation of MIR harmonics was also observed [9]. Shown in Fig. 10 is the harmonic-continuum generation in the third harmonic in a GaAs(100) crystal (350 μm thick). If we compare the previous theoretical calculation of the spectral broadening of the third harmonic (see Fig. 3) with the experiment we see that the spec-

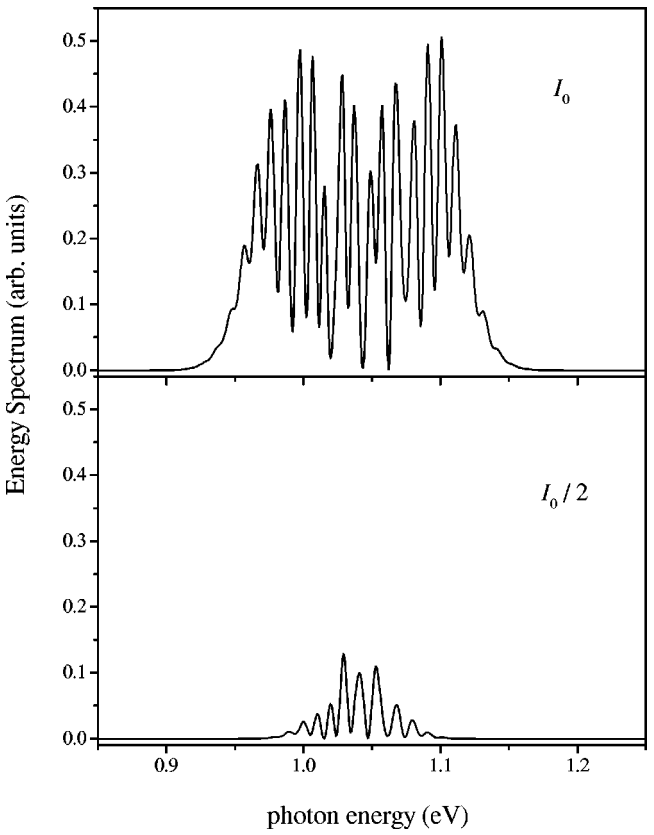

FIG. 11. Theoretical energy spectrum in the third harmonic for different pulse intensities I_0 and $I_0/2$. The same parameters as in Fig. 10 are used. SPM and pulse splitting have been considered.

tral broadening is qualitatively reproduced. However, the calculations fail to explain the periodic spectral modulation. It has been observed that an ultrafast pulse undergoes pulse splitting for input powers that are above a critical power [6,21]. This effect is a combination of self-focusing and group-velocity dispersion and is thought to arrest catastrophic self-focusing. Therefore, we perform calculations for this higher intensity and shorter MIR pulse, assuming that the fundamental MIR pulse consists of two temporally separated pulses:

$$A_1(0,t)^2 = \frac{A_0^2}{1+r}\left[\frac{r}{\cosh[(t+t_0)/T]} + \frac{1}{\cosh[(t-t_0)/T]}\right], \tag{3.1}$$

where $2t_0$ is the pulse separation and r the ratio between the two peaks. Assuming the fundamental pulses are separated by $t_0 \simeq \Delta = 200$ fs with a ratio $r \simeq 1.55$, the calculation qualitatively matches the experimental data, as shown in Fig. 11. A smaller pulse splitting effect is expected as the intensity decreases. Therefore, we assume for the smaller intensity case, $I_0/2$, a pulse separation $t_0 \simeq 182$ fs. In agreement with the experiment the frequency shift becomes smaller as the pulse intensity decreases while the periodicity of the peaks increases as the intensity decreases. The spectral modulation is due primarily to pulse splitting in the fundamental, which translates into pulse splitting in the third harmonic. Spectral interference between the time separated pulses ($\simeq 400$ fs between third-harmonic pulses at intensity I_0) produces the periodic spectral modulation. The asymmetry in the two peaks produces modulation in the energy spectrum that does not reach zero. The resulting spectral width in the third harmonic is due to SPM in the fundamental being mapped onto the third harmonic via XPM. The spectral modulation is due to spectral interference from each of the split pulses in the third harmonic, formed from the split pulses in the fundamental during propagation. This result suggests that this process is a result of self-phase-modulation and pulse splitting in the fundamental in combination with good phase matching to generate the third harmonic.

IV. CONCLUSIONS

We used a multiple-order perturbation theory based on the set of coupled nonlinear wave equations to describe the effect of self-phase-modulation on multiple-order nonlinear phenomena. We found that SPM induced in the initial field can play an important role in the phenomena. For example, we found that spectral broadening occurs in the harmonic fields and is due to the spectral broadening of the fundamental beam being mapped onto the harmonic during propagation via cross-phase modulation. We also found that SPM alleviates phase mismatch in multiple harmonic generation and multiple off-resonance optical-sideband generation in the presence of SPM. This occurs because additional bandwidth in the fundamental due to SPM provides a distribution of wave vectors that aids in the generation of multiple harmonics or sidebands. We also found that SPM could lead to a harmonic or sideband bandwidth larger than what is usually expected.

We compared the theoretical results with recent experiments in multiple-order nonlinear phenomena induced by intense mid-infrared pulses in semiconductors. We obtained good agreement between the calculations and the experimental data under most of the conditions explored. In order to reproduce the spectral modulation and broadening found in harmonics at higher intensity with subpicosecond MIR pulses, we had to assume temporal separation (or pulse splitting) in the fundamental MIR occurs, which is expected to occur under those experimental conditions.

ACKNOWLEDGMENTS

We gratefully acknowledge support from NSF Grant No. DMR-0049024, ONR Grant No. N00014-94-1-1024, the Japan Science and Technology Corporation PRESTO Program, and the NEDO International Joint Research Grant Program. O.G.C. is supported by Becas Complutense ''del Amo.'' We thank Dr. T. Kimura for his help with the setup of the laboratory, A. P. Mitchell and J. Guo for their help with data collection, and Professor H. A. Schwettman and Professor T. I. Smith for their encouragement and support. A.H.C. wishes to thank Dr. C. V. Bennet for fruitful discussions.

[1] R. R. Alfano and S. L. Shapiro, Phys. Rev. Lett. **24**, 584 (1970); **24**, 592 (1970).
[2] G. Y. Yang and Y. R. Shen, Opt. Lett. **9**, 510 (1984).
[3] F. A. Ilkov, L. Sh. Ilkova, and S. L. Chin, Opt. Lett. **18**, 681 (1993).
[4] For example, M. K. Reed, M. K. Steiner-Shepard, M. S. Armas, and D. K. Negus, J. Opt. Soc. Am. B **12**, 2229 (1995).
[5] A. Brodeur and S. L. Chin, Phys. Rev. Lett. **80**, 4406 (1998).
[6] J. K. Ranka, R. W. Schirmer, and A. L. Gaeta, Phys. Rev. Lett. **77**, 3783 (1996).
[7] A. L. Gaeta, Phys. Rev. Lett. **84**, 3582 (2000).
[8] N. I. Koroteev and A. M. Zheltikov, Appl. Phys. B: Lasers Opt. **67**, 53 (1998).
[9] A. H. Chin, O. G. Calderón, and J. Kono, Phys. Rev. Lett. (to be published).
[10] R. Zürl and H. Graener, Appl. Phys. B: Lasers Opt. **66**, 213 (1998).
[11] T. Tsang, Phys. Rev. A **54**, 5454 (1996).
[12] B. Sheehy, J. D. D. Martin, L. F. DiMauro, P. Agostini, K. J. Schafer, M. B. Gaarde, and K. C. Kulander, Phys. Rev. Lett. **83**, 5270 (1999).
[13] L. Nugent-Glandorf, M. Scheer, M. Krishnamurthy, J. W. Odom, and S. R. Leone, Phys. Rev. A **62**, 023 812 (2000).
[14] Y. B. Band, Phys. Rev. A **42**, 5530 (1990).
[15] H. J. Bakker, P. C. M. Planken, L. Kuipers, and A. Lagendijk, Phys. Rev. A **42**, 4085 (1990).
[16] Y. B. Band, C. Radzewicz, and J. S. Krasinski, Phys. Rev. A **49**, 517 (1994).
[17] G. P. Agrawal, P. L. Baldeck, and R. R. Alfano, Phys. Rev. A **40**, 5063 (1989).
[18] R. R. Alfano, Q. Z. Wang, T. Jimbo, P. P. Ho, R. N. Bhargava, and B. J. Fitzpatrick, Phys. Rev. A **35**, 459 (1987).
[19] R. W. Boyd, *Nonlinear Optics* (Academic Press, San Diego, 1992).
[20] P. N. Butcher and D. Cotter, *The Elements of Nonlinear Optics* (Cambridge University Press, New York, 1990).
[21] A. A. Zozulya, S. A. Diddams, A. G. Van Engen, and T. S. Clement, Phys. Rev. Lett. **82**, 1430 (1999).